FULL PAPER

ADVANCED FUNCTIONAL MATERIALS

DOI: 10.1002/adfm.200600568

A Hierarchically Structured $Ni(OH)_2$ Monolayer Hollow-Sphere Array and Its Tunable Optical Properties over a Large Region**

By *Guotao Duan*, *Weiping Cai*,* *Yuanyuan Luo*, and *Fengqiang Sun*

The fabrication of a hierarchically structured $Ni(OH)_2$ monolayer hollow-sphere array with the shell composed of building blocks of nanoflakelets is demonstrated based on a colloidal monolayer and electrochemical deposition. The morphology can be easily controlled by the colloidal monolayer and deposition parameters. Importantly, such monolayer hollow-sphere array shows a morphology- and size-dependent tunable optical transmission stop band. This stop band can be easily tuned from 455–1855 nm by changing the size of the hollow spheres between 1000 and 4500 nm, and also fine-adjusted by changing the deposition time. The array exhibits a nearly incident-angle-independent position of the stop band that 3D photonic crystals do not possess. This structure may have potential applications in optical devices, photonic crystals, and sensors for gas detection.

1. Introduction

Hollow-sphere structures, ranging from carriers and containers[1,2] to microreactors,[3,4] have recently received considerable attention because of their novel interior geometry and surface functionality.[1–14] This allows many applications in drug delivery,[7] food and cosmetic industries,[8] biotechnology,[9] photocatalysts,[10] and photonic devices.[11] The success of these applications strongly relies on the material and the size of the hollow sphere, and also on the fine structure of the spherical shells. Hierarchically structured hollow spheres with the shell composed of nanosized building blocks (e.g., nanoparticles, nanorods, or nanosheets) should be of great importance to the next generation of nanodevices. Recently, fabrication of hierarchically structured nanoarchitectures has been a research hotspot. By a mild hydrothermal process, some groups have fabricated various hierarchically structured hollow spheres with nanoparticles, nanorods, or nanosheets as building blocks.[15–20] However, the work on morphology- and size-controlled formation needs to be continued for novel properties and applications.

In the past years, patterned arrays induced by colloidal-monolayer lithography have received much attention, due to their potential applications in catalysis, photonic crystals, and optoelectronic devices.[21–29] It is important in the design of novel nanodevices to assemble hierarchically structured hollow spheres into ordered arrays, since such organized structures combine the merits of nanosized materials and patterned arrays. However, besides hierarchical porous arrays,[11] there are few reports of hollow-sphere arrays where the shells are composed of 1D or 2D fine nanostructures.

Here, we report the fabrication of hierarchical $Ni(OH)_2$ monolayer hollow-sphere arrays with a fine structure of nanoflakelets by an electrochemical strategy based on a polystyrene (PS) sphere colloidal monolayer. The structure and morphology can easily be controlled. Importantly, under perpendicular incidence of a light beam, such hierarchically structured hollow-sphere arrays have demonstrated a tunable optical transmission stop band in the visible–near-IR (vis–NIR) region from 455–1855 nm, depending on the hollow-sphere size and the fine structure. The arrays exhibit a nearly incident-angle-independent position of the stop band, which 3D photonic crystals do not possess. This should be of great significance for applications in optical devices, photonic crystals, nanoscience, and nanotechnology.

2. Results and Discussion

2.1. Hierarchically Structured Monolayer Hollow-Sphere Arrays

Based on a PS colloidal monolayer on indium tin oxide (ITO) glass and electrochemical deposition in 1 M $NiNO_3$, a $Ni(OH)_2$ monolayer hollow-sphere array can be obtained. Figure 1A–C shows the morphology of the as-prepared samples (different size of PS for Fig. 1A and 1C) after removal of the PS monolayer by dissolution in CH_2Cl_2. It can be seen that the microspheres are uniformly packed into an array with hexagonal symmetry. The periodicity, i.e., the central distance between

[*] Prof. W. Cai, G. Duan, Y. Luo, Dr. F. Sun
Key Lab of Materials Physics, Anhui Key Lab of Nanomaterials and Nanotechnology, Institute of Solid State Physics
Chinese Academy of Sciences
Hefei, Anhui, 230031 (P.R. China)
E-mail: wpcai@issp.ac.cn

[**] The authors acknowledge the financial support from the National Natural Science Foundation of China (Grant No. 50502032), Natural Science Foundation of the Anhui Province (Grant No. 050440902), and the Major State research program of China "Fundamental Investigation on Micro-Nano Sensors and Systems based on BNI Fusion" (Grant No. 2006CB300402). The authors also thank one of the referees of this article for his good suggestions that made this work progress further.

ADVANCED FUNCTIONAL MATERIALS

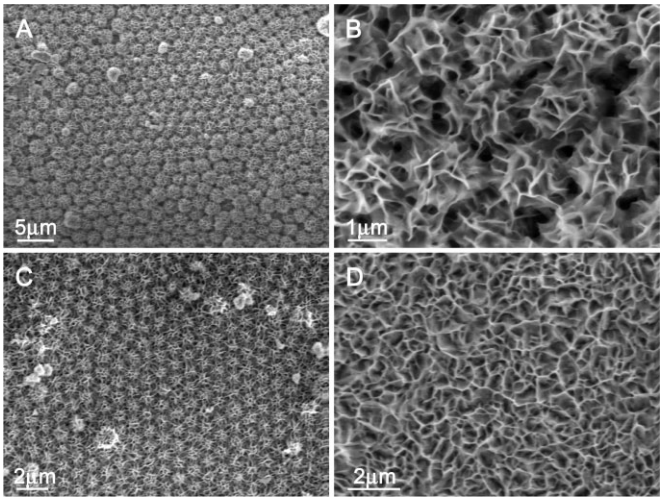

Figure 1. Typical FE-SEM images of the as-deposited samples. The size of the PS spheres and the deposition time are A) 2 μm and 100 min, and C) 1 μm and 60 min, respectively. D) No PS spheres used and 60 min deposition time, B) a local enlarged image of A.

the adjacent spheres in the array, can be controlled by the size of the PS used (see Fig. 1A and C). The local magnification shows that the spheres in the array have a hierarchical structure (see Fig. 1B). The spheres are composed of massive ultrathin sheets or nanoflakelets (or nanowall) nearly vertical to the spherical surface, showing high specific surface area. For reference, electrochemical deposition was also carried out on the ITO-glass substrate without the PS template, showing only a film consisting of net- or wall-like arranged nanoflakelets (nearly vertical standing) (see Fig. 1D). The corresponding X-ray diffraction (XRD) spectra show that the as-deposited samples are α-nickel hydroxide with lattice parameters $a = 3.09$ Å and $c = 22.11$ Å (as shown in Fig. 2).

For determination of the structural formula of such α-nickel hydroxide, IR spectra and thermogravimetric analysis (TGA) were carried out on the as-deposited monolayer hollow-sphere

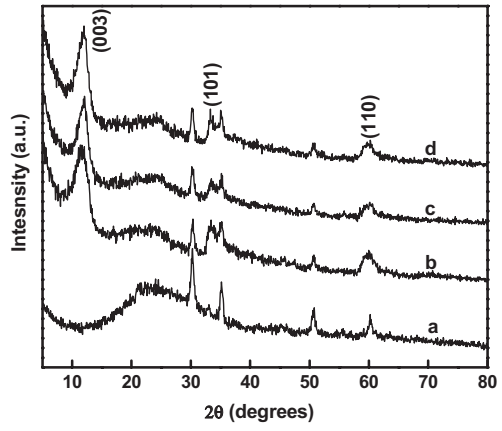

Figure 2. XRD spectra of ITO-glass (curve a) and the as-deposited samples (curves b–d). The PS sphere size and the deposition time are b) no PS used and 60 min, c) 1 μm and 60 min, and d) 2 μm and 100 min, respectively (indexes correspond to α-$Ni(OH)_2$).

array based on PS (2 μm in diameter) colloidal monolayer (deposition time: 100 min). The corresponding measurements are shown in Figure 3 and Figure 4. The IR spectrum includes i) a broad peak centered around 3420 cm^{-1} corresponding to interlamellar water and OH-bond vibration, ii) absorption at

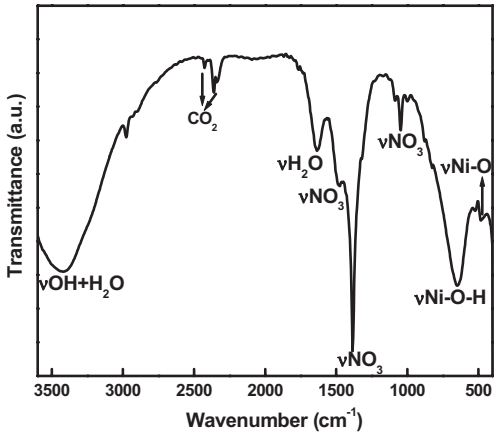

Figure 3. IR spectrum of the as-deposied $Ni(OH)_2$ hollow-sphere array based on a PS (2 μm in diameter) colloidal monolayer (deposition time: 100 min).

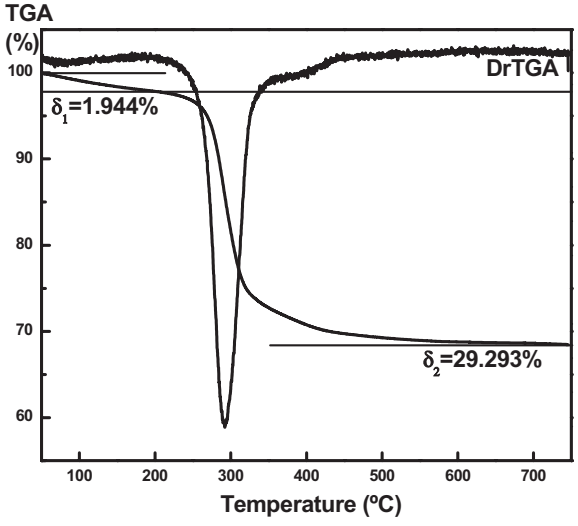

Figure 4. TGA curve of the sample corresponding to Figure 3.

2424 and 2356 cm^{-1} due to CO_2 in air, iii) absorptions in the range of 1000–1500 cm^{-1} due to intercalated anions NO_3^-, and iv) absorptions at 648 and 485 cm^{-1} due to the Ni–O–H bending and Ni–O stretching vibrations, respectively. Then the composition of the hollow spheres can be marked with the approximate formula $Ni(OH)_x(NO_3)_{2-x}{\cdot}yH_2O$,[30] in which the values of x and y can be determined from the TGA curve as $x = 1.693$ and $y = 0.117$,[30] so the formula becomes $Ni(OH)_{1.693}(NO_3)_{0.307}{\cdot}0.117H_2O$.

Transmission electron microscopy (TEM) examination shows that the microspheres are hollow in interior (see

Fig. 5A), which means that the shell layer of the sphere consists of incompact-arranged nanoflakelets. The selected-area electron diffraction (SAED) pattern reveals that the flakelet is not an intact single crystal because of weak diffraction rings

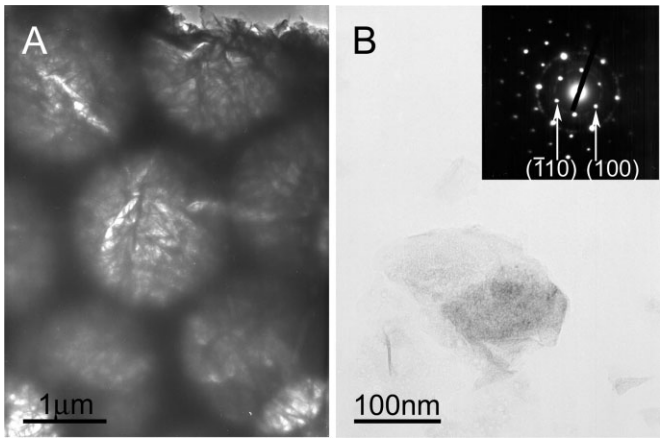

Figure 5. TEM images of the as-deposited sample shown in Figure 1A. A) Detached layer of the hollow-sphere array, B) a single nanoflakelet. Inset in B: SAED pattern corresponding to B.

penetrating the diffraction spots, according to the nature of α-$Ni(OH)_2$.[20] However, both the diffraction spots and rings show that the flakelet has an orientation with the planar surface perpendicular to the *c*-axis (see inset in Fig. 5B).

The hollow structure can more clearly be seen in the edge region of the sample shown in Figure 1A, as illustrated in Figure 6. There are many broken hollow spheres. Also, we can see that $Ni(OH)_2$ grows both on the place of the substrate without PS and along PS in the PS colloidal monolayer. Such hollow-

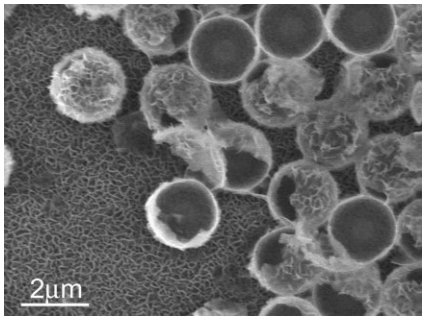

Figure 6. FE-SEM image in the edge region for the sample shown in Figure 1A.

sphere monolayer can be detached from the substrate by a blade, as illustrated in Figure 7A, corresponding to the sample in Figure 1A and partial disconnection of the hollow-sphere monolayer. After detachment of the hollow-sphere layer, a layer of $Ni(OH)_2$ with bowl-like pore array is left on the ITO substrate because of the geometry of polystyrene (see Fig. 7B). Obviously, the thickness of the pore array is much smaller than

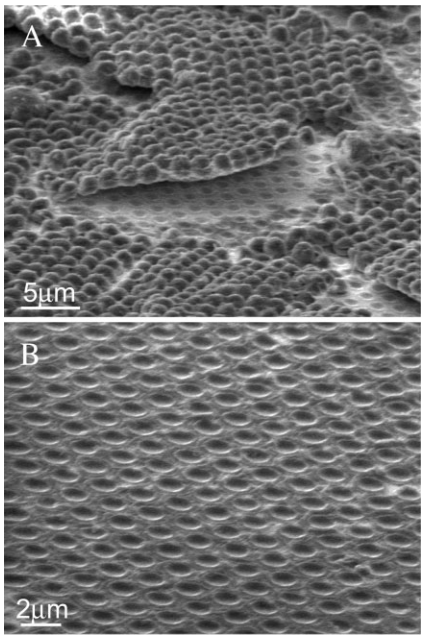

Figure 7. FE-SEM images of the sample shown in Figure 1A with A) partial detachment and B) after full detachment of the hollow-sphere array.

the radius of the PS spheres, indicating that the growth on ITO will be depressed after formation of a net-like film in the presence of the PS colloidal monolayer.

Further experiment reveals that the deposition time is very important to form the hollow-sphere arrays with hierarchical structure, as shown in Figure 8. For the template with PS spheres of 2 μm, a short deposition time (30 min) only induces

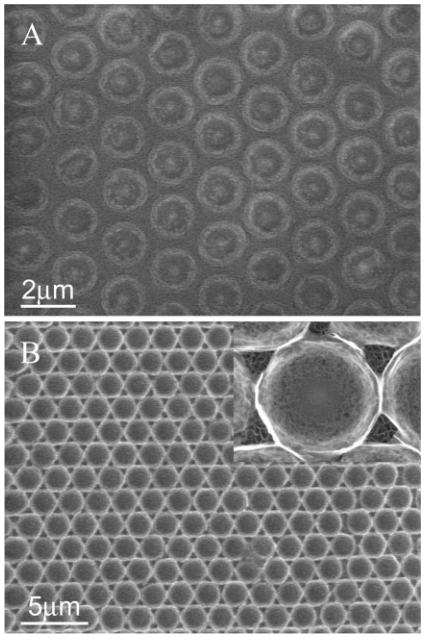

Figure 8. FE-SEM images of ordered $Ni(OH)_2$ arrays based on a PS (2 μm in diameter) colloidal monolayer. The deposition times are A) 30 min, B) 50 min.

a ring-like array of $Ni(OH)_2$ on the ITO substrate (see Fig. 8A), meaning nucleation and growth starts at the sites between the PS spheres and the substrate. Increasing the deposition time to 50 min, an ordered bowl-like pore array was formed (see Fig. 8B). We can also see the net-like film at the interstitial sites among the PS spheres (inset of Figure 8B), which demonstrated that the film growth on the ITO substrate was finished before the complete formation of hollow spheres. After formation of the hollow-sphere array, when further increasing the deposition time, the shell of the hollow spheres become denser with more nanoflakelets. In addition, it is shown that the formation of hollow, structured spheres was sensitive to the cathodic deposition current density (J). With J increasing from 1.2 to 2.0 mA cm^{-2}, a uniform hollow-sphere array cannot be obtained but only an aggregation of nanoflakelets is obtained (see Fig. 9). Also, too small deposition current densities are not appropriate due to the low deposition efficiency.

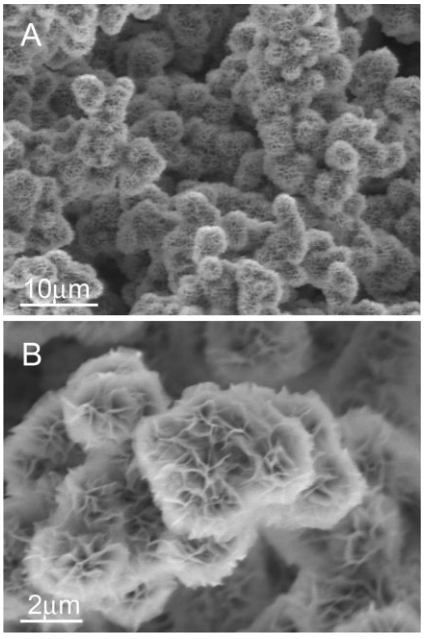

Figure 9. A) FE-SEM images of a $Ni(OH)_2$ hierarchical structure electrodeposited with a cathodic current density 2 mA cm^{-2} and 100 min without template; B) local image of (A). The existence of a PS colloidal monolayer also shows a similar morphology. Even when decreasing the deposition time a hollow-sphere array can still not be obtained at this cathodic current density.

2.2. Formation Mechanism

Formation of α-$Ni(OH)_2$ by electrochemical reaction was studied in earlier work.[30,31] The metal Ni^{2+} ions in the solution react with OH^-, which was produced by the reduction of NO_3^- close to the cathode, forming $Ni(OH)_2$, according to the following reactions:

$$NO_3^- + H_2O + 2e^- \rightarrow NO_2^- + 2\,OH^- \quad (1)$$

$$Ni^{2+} + 2\,OH^- \rightarrow Ni(OH)_2 \quad (2)$$

In the reaction process, Ni cannot form because the reaction potential of Ni^{2+} to Ni is much more negative than that of NO_3^- to NO_2^- (–0.23 V versus 0.01 V).[31] It has been reported that negatively charged PS can be covered with a smooth inorganic layer by the hydrolysis of metal ions.[32] The PS used in our experiment was also negatively charged. The $Ni(OH)_2$ formed by Equations 1 and 2 will subsequently deposit or nucleate on both the ITO substrate and the interstitial sites between the PS and the substrate. For the latter, deposition along the PS surface takes place, leading to a final spherical shell, as schematically illustrated in Figure 10.

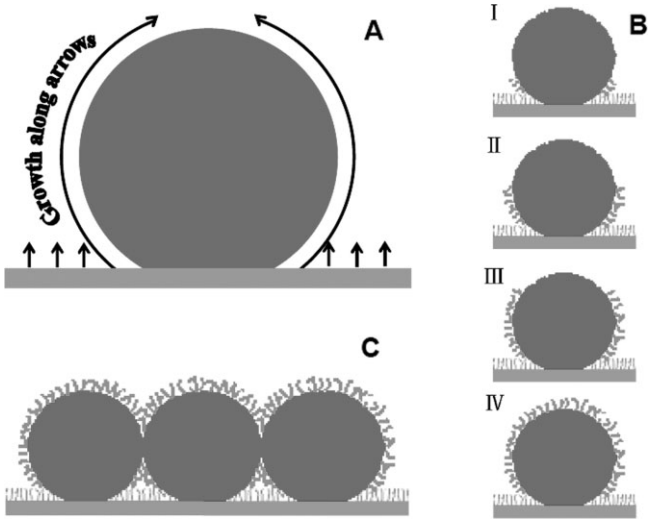

Figure 10. Schematic illustration for the formation of a hierarchical $Ni(OH)_2$ hollow-sphere array. A,C) schematic initial and final state, respectively; B) schematic growth process.

Since the $Ni(OH)_2$ crystal has a layered structure of the CdI_2 type, which shows the weak interaction between layers and the strong binding within the layered planes, that is, the surface energy of the layered (001) plane is the lowest. Nickel hydroxide will preferentially grow along the layered plane after the formation of its nuclei. Also, due to the directional deposition under the electrical potential, only nuclei oriented with their (001) plane vertical to the substrate and the PS surface will grow preferentially, leading to the final formation of a wall-like fine structure of $Ni(OH)_2$ nanoflakelets nearly vertical to the substrate and the PS surface (see Fig. 10). It should be mentioned here that partial NO_3^- anions and H_2O molecules will be inserted into the $Ni(OH)_2$ layers during electrodeposition, forming the α-type structure.

As for the effect of J, obviously, a high J value is non-beneficial to the preferential deposition due to the fast deposition rate. In the case of $J = 2.0$ mA cm^{-2}, homogeneous nucleation takes place close to the electrode, and as such $Ni(OH)_2$ grew into the aggregation of nanoflakelets without hollow spheres (see Fig. 9).

2.3. Tunable Optical Transmission Stop Band

The prepared monolayer hollow-sphere array demonstrates tunable optical properties in a large region. Figure 11 shows optical transmission spectra with the incident light aligned perpendicularly to the as-prepared $Ni(OH)_2$ samples on ITO. A size-dependent optical transmission stop band exists in the

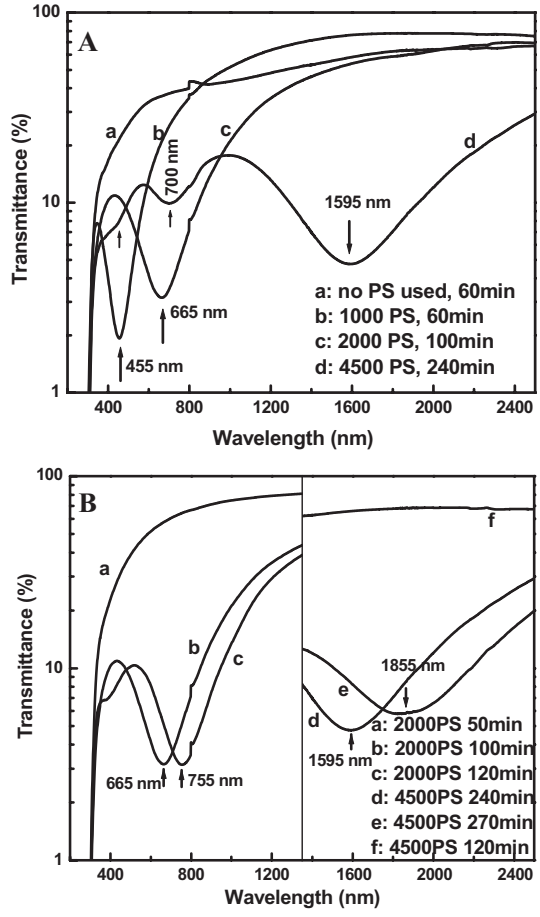

Figure 11. Optical transmission spectra of $Ni(OH)_2$ samples on ITO glass with the incident light perpendicular to the substrate.

hierarchically structured hollow-sphere arrays, which red-shifts in over a large range from 455–1595 nm with an increase in size of the hollow spheres in the array from 1000–4500 nm. For the hollow-sphere array based on the 4500 nm PS spheres, in addition to the main stop band around 1595 nm, there is another weaker band located around 700 nm together with a shoulder at 450 nm. As we know, the periodicity of the array is controlled by the size of the PS spheres, we can thus easily adjust the optical transmission stop band in a large region from the visible to near-IR region simply by changing the size of the PS spheres. In contrary, no such stop band is detected for the net-like film (see curve a in Fig. 11 A corresponding to the sample shown in Fig. 1D), or for the hierarchically structured pore array (see curves a and f in Fig. 11B). This demonstrates that the monolayer hollow-sphere structured array is crucial to produce such tunable optical bands.

Interestingly, the position of the stop band can also be fine-adjusted by tuning the deposition time without changing the periodicity. An increase of the deposition time leads to a red-shift of the band for the hollow-sphere arrays, as shown in curves b–e of Figure 11B, which could be due to the denser shell of the hollow sphere. It means that we can very flexibly control the optical transmission stop band in a large region, by controlling the size of the PS spheres for coarse tuning and changing the deposition time for fine adjusting, which is undoubtedly important both in applications and in fundamental research.

Further experiments show that the position of the transmission stop band is almost independent of the incident angle θ (the angle between the incident light beam and the normal to the sample plane). For the monolayer hollow-sphere array based on the PS monolayer with 2000 nm spheres, the center of the transmission stop band red-shifts less than 30 nm with a change in the incident angle from 0° to 75°, as shown in Figure 12. This is quite small and almost negligible compared to the changes observed for the stop band in 3D photonic crystals, which is very sensitive to θ according to[33–35]

$$m\lambda_{\min} = 2d(n^2 - \sin^2\theta)^{1/2} \quad (3)$$

where m is the order of the diffraction, $\lambda_{\min}$ is the wavelength of the stop band, n is the mean refraction index of the 3D crystal, and d is the periodical constant along the normal of the sample plane. It is well known that the θ-dependence of the position of the stop band is a disadvantage of 3D photonic crystals in applications. If one wants to prevent transmission of light from any incident angle, a full photonic crystal with a θ-independent stop band is needed. This is a challenge for 3D photonic crystals. The monolayer hollow-sphere array attained

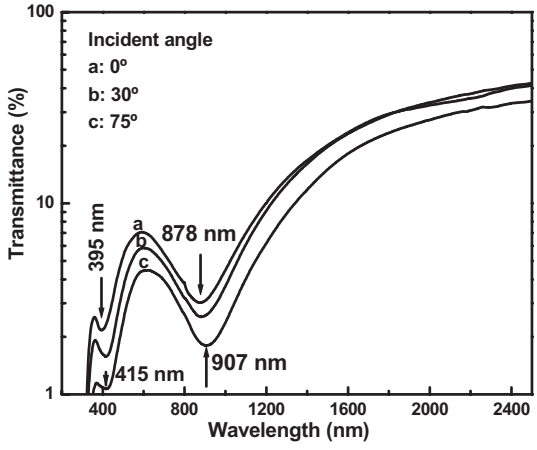

Figure 12. Optical transmission spectra of a $Ni(OH)_2$ sample on ITO glass with different incident angles (the angle between the incident light and the normal to the sample plane, θ). The sample was prepared by electrodeposition with $J = 1.2$ mA cm^{-2} for 140 min based on a 2000 nm size spheres PS monolayer. It has two clear transmission stop bands because of first and second diffractions, which is beneficial to the understanding of the shift of stop band.

here could be a good candidate for this kind of applications as it shows a θ-independent stop band.

2.4. Equivalent Double-Layer Photonic Crystals

Generally, an optical transmission stop band will be found in 3D colloidal crystals (or inverse opal structures) but cannot be produced in a 2D monolayer colloidal crystal. The monolayer hollow-sphere array in our case, however, can equivalently be considered as symmetrical double layers (top layer and bottom layer) with inter-spacing d, as shown in Figure 13, indicating a photonic crystal with two layers. Under perpendicular incidence of a light beam (or $\theta = 0$, see Figure 13 A) Equation 3 can be written as $m\lambda_{min} = 2nd$, where n corresponds to the mean refractive index of the layers (consisting of sphere shell and interstice). Although the exact values of n and d are unknown, the d value should increase with a rise in the size of the PS spheres, and n depends on the material species and structure of the shell. Obviously, the denser the sphere shell (or the longer the deposition time), the larger the n value. Thus, for the first-order diffraction ($m = 1$), the transmission stop band should red-shift with an increase in sphere size or deposition time (see Fig. 11). Also, there should be a multiple relation between different diffraction orders ($m = 1, 2, 3$), which is in rough agreement with the results (see curve d in Fig. 11). The slight deviation may originate from wavelength-dependent optical absorption of the $Ni(OH)_2$, which superimposes on the transmission spectra and hence changes the measured band position.

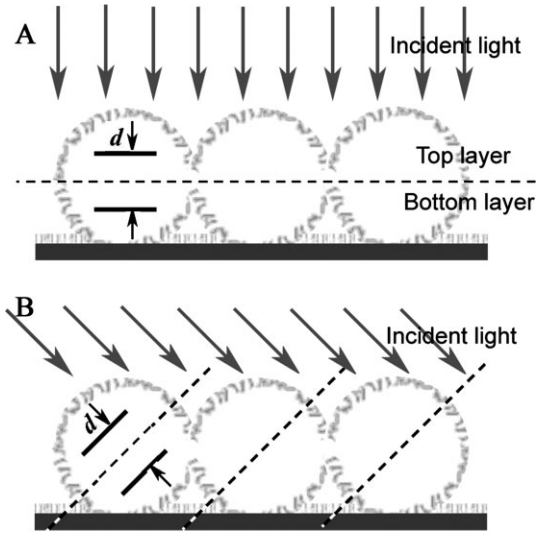

Figure 13. Schematic illustration of the double-layer photonic crystal approximation for the hollow-sphere array. A) Incidence of light perpendicular to the sample plane ($\theta = 0$); B) aslant incidence of light ($\theta > 0$)

As for the θ-independent stop band, it can be attributed to the special structure of the hollow-sphere monolayer. Because of the symmetry of the hollow spheres, for incident light with different θ values, the d value should be similar (see Fig. 13B) and thus the position of the stop band is almost independent of θ.

3. Conclusions

We have demonstrated a hierarchical $Ni(OH)_2$ monolayer hollow-sphere array with the shells composed of massive nanoflakelets by an electrochemical strategy based on a colloidal monolayer. Such hierarchical hollow-sphere array shows a tunable optical transmission stop band in the vis–NIR region. It can easily be tuned in a large region by the choice of PS sphere size, and also fine-adjusted by adjusting the deposition time. Importantly, this monolayer hollow-sphere array exhibits a nearly incident-angle-independent position of the stop band, which 3D photonic crystals do not possess. This hollow-sphere-array structure that has been prepared by a low-cost and facile method in a controlled process combines the merits of both patterned arrays and nanocrystals (or nanoflakelets), and maybe useful for a wide variety of potential applications in optical devices, photonic crystals, nanoscience, and nanotechnology. Among them could be a prime candidate of a full photonic crystal with a θ-independent stop band.

Since the position of the stop band is associated with n, the factors influencing the n value will lead to a position change of stop band. In our case, the hollow spheres with the shells composed of massive nanoflakelets possess a high specific surface area. Adsorption of environmental gases will occur on the surface of nanoflakelets, which will lead to a change of the n value and hence a shift of the stop band. It means that such monolayer hollow-sphere array with hierarchical structure could be a good optical gas-sensor. Preliminary experiments have confirmed a significant shift of the stop band induced by exposure to an alcohol atmosphere, and such shift can be recovered completely by subsequent heating at 100 °C in air (see Fig. 14). Alternate exposure and heating show a reversible shift of the band. Further work is in progress and will be reported on later. It is because of the $Ni(OH)_2$ present that we can produce the hollow spheres with nanoflakelets. The monolayer hollow-

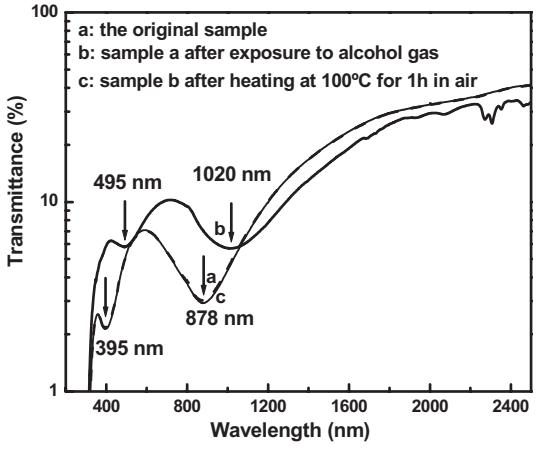

Figure 14. Optical transmission spectra for the sample shown in Figure 12, with the incident light perpendicular to the substrate. After exposure of the original sample to alcohol gas (in a sealed cup with alcohol) for 30 min, the first and second stop bands red-shift more than 140 nm and 100 nm, respectively (curve b). After subsequent heating at 100 °C for 1 h in air (curve c), the bands can be recovered completely.

sphere array with hierarchical structure provides the practical possibility of a new optical sensor for gas detection.

4. Experimental

Polystyrene (1 μm, 2 μm, and 4.5 μm in diameters) suspensions were bought from Alfa Aesar Corporation. Glass substrates were cleaned according to previously published procedures [21]. A 1 cm^2 sized ordered colloidal monolayer was synthesized on the glass substrates by spin-coating with a custom-built spin coater. Some ITO-glass substrates were ultrasonically cleaned in acetone, ethanol, and distilled water for 30 min each. The monolayer on the glass substrate was integrally lifted off and floated on the surface of distilled water in a cup, after which it could be picked up using the ITO-glass substrate, as previously illustrated [25], followed by heating at 110 °C in an oven for 2 min to bond the monolayer with the ITO substrate. The edges of the monolayer on the ITO were covered by an aluminum frame and insulating tape, and immersed into an electrolyte solution as a working electrode. The electrolyte was composed of 1 M $Ni(NO_3)_2$ aqueous solution and its pH value was adjusted to 1.7 with nitric acid. A cleaned polycrystalline nickel sheet was used as the auxiliary electrode. The distance between the working electrode and the auxiliary electrode was about 6 cm. The electrodeposition was carried out at 60 °C with a cathodic current density of 1.2 mA cm^{-2}. After deposition, the monolayer was removed by dissolution in CH_2Cl_2, and an ordered $Ni(OH)_2$ hollow-sphere array was thus obtained and characterized before heat treatment at 100 °C for 1 h.

The as-prepared samples were examined by field-emission scanning electron microscopy (FE-SEM) (Sirion 200) and TEM (JEM-200CX). X-ray diffraction (XRD) was measured on a Philips X'Pert using Cu Kα radiation ($\lambda = 0.15419$ nm). TGA was carried out on a TA-50 thermal analyzer (Shimadzu) with a heating rate of 10 °C min^{-1}. IR transmission spectra were measured on a Nicolet model Imapact 400D FTIR spectrometer (KBr pellets, 4 cm^{-1} resolution). The optical transmission spectra were recorded at room temperature on a Cary 5E UV-vis–NIR spectrophotometer in the wavelength range of 200–2500 nm.

Received: June 28, 2006
Revised: September 15, 2006
Published online: January 24, 2007

[1] D. G. Shchukin, G. B. Sukhorukov, *Langmuir* **2003**, *19*, 4427.
[2] G. Ibarz, L. Dähne, E. Donath, H. Möhwald, *Adv. Mater.* **2001**, *13*, 1324.
[3] D. G. Shchukin, I. L. Radtchenko, G. B. Sukhorukov, *ChemPhysChem* **2003**, *4*, 1101.
[4] D. G. Shchukin, G. B. Sukhorukov, *Adv. Mater.* **2004**, *16*, 671.
[5] F. Caruso, R. A. Caruso, H. Möhwald, *Science* **1998**, *282*, 1111.
[6] W. Meier, *Chem. Soc. Rev.* **2000**, *29*, 295.
[7] Y. Zhu, J. Shi, W. Shen, X. Dong, J. Feng, M. Ruan, Y. Li, *Angew. Chem. Int. Ed.* **2005**, *44*, 5083.
[8] D. G. Shchukin, G. B. Sukhorukov, H. Möhwald, *Angew. Chem. Int. Ed.* **2003**, *42*, 4472.
[9] D. G. Shchukin, A. A. Patel, G. B. Sukhorukov, Y. M. Lvov, *J. Am. Chem. Soc.* **2004**, *126*, 3374.
[10] D. G. Shchukin, R. A. Caruso, *Chem. Mater.* **2004**, *16*, 2287.
[11] L. Lu, R. Capek, A. Kornowski, N. Gaponik, A. Eychmüller, *Angew. Chem. Int. Ed.* **2005**, *44*, 5997.
[12] Y. D. Yin, R. M. Rioux, C. K. Erdonmez, S. Hughes, G. A. Somorjai, A. P. Alivisatos, *Science* **2004**, *304*, 711.
[13] X. Sun, Y. Li, *Angew. Chem. Int. Ed.* **2004**, *43*, 3827.
[14] S. H. Im, U. Jeong, Y. Xia, *Nat. Mater.* **2005**, *4*, 671.
[15] B. Liu, H. C. Zeng, *J. Am. Chem. Soc.* **2004**, *126*, 8124.
[16] B. Liu, H. C. Zeng, *J. Am. Chem. Soc.* **2004**, *126*, 16 744.
[17] J. Li, H. C. Zeng, *Angew. Chem. Int. Ed.* **2005**, *44*, 4342.
[18] Z. Zhang, X. Shao, H. Yu, Y. Wang, M. Han, *Chem. Mater.* **2005**, *17*, 332.
[19] M. Mo, J. C. Yu, L. Zhang, S.-K. A. Li, *Adv. Mater.* **2005**, *17*, 756.
[20] D. Wang, C. Song, Z. Hu, X. Fu, *J. Phys. Chem. B* **2005**, *109*, 1125.
[21] C. L. Haynes, R. P. Van Duyne, *J. Phys. Chem. B* **2001**, *105*, 5599.
[22] M. A. Ghanem, P. N. Bartlett, P. de Groot, A. Zhukov, *Electrochem. Commun.* **2004**, *6*, 447.
[23] X. Che, Z. Chen, N. Fu, G. Lu, B. Yang, *Adv. Mater.* **2003**, *15*, 1413.
[24] P. N. Bartlett, J. J. Baumberg, S. Coyle, M. E. Abdelsalam, *Faraday Discuss.* **2004**, *125*, 117.
[25] F. Sun, W. Cai, Y. Li, B. Cao, Y. Lei, L. Zhang, *Adv. Funct. Mater.* **2004**, *14*, 283.
[26] F. Sun, W. Cai, Y. Li, B. Cao, F. Lu, G. Duan, L. Zhang, *Adv. Mater.* **2004**, *16*, 1116.
[27] J. M. McLellan, M. Geissler, Y. Xia, *J. Am. Chem. Soc.* **2004**, *126*, 10 830.
[28] S. Han, X. Shi, F. Zhou, *Nano Lett.* **2002**, *2*, 97.
[29] G. Duan, W. Cai, Y. Li, Z. Li, B. Cao, Y. Luo, *J. Phys. Chem. B* **2006**, *110*, 7184.
[30] R. S. Jayashree, P. V. Kamath, *J. Appl. Electrochem.* **1999**, *29*, 449.
[31] G. H. A. Therese, P. V. Kamath, *Chem. Mater.* **2000**, *12*, 1195.
[32] H. Shiho, N. Kawahashi, *Colloid Polym. Sci.* **2000**, *278*, 270.
[33] H. Fudouzi, Y. Xia, *Langmuir* **2003**, *19*, 9653.
[34] A. Richel, N. P. Johnson, D. W. McComb, *Appl. Phys. Lett.* **2000**, *77*, 1062.
[35] R. Mayoral, J. Requena, J. S. Moya, C. López, A. Cintas, H. Miguez, F. Meseguer, L. Vázquez, M. Holgado, Á. Blanco, *Adv. Mater.* **1997**, *9*, 257.